Nanoscale

PAPER

View Article Online
View Journal | View Issue

Cite this: *Nanoscale*, 2023, **15**, 9745

Vertically oriented self-assembly of colloidal CdSe/CdZnS quantum wells controlled *via* hydrophilicity/lipophilicity balance: optical gain of quantum well stacks for amplified spontaneous emission and random lasing†

Zeynep Dikmen, [a,b] Ahmet Tarık Işık,[b] İklim Bozkaya,[b] Hamed Dehghanpour Baruj, [b] Betül Canımkurbey, [b,c] Farzan Shabani,[b] Muhammad Ahmad[b] and Hilmi Volkan Demir *[b,d]

We propose and demonstrate vertically oriented self-assembly of colloidal quantum wells (CQWs) that allows for stacking CdSe/CdZnS core/shell CQWs in films for the purposes of amplified spontaneous emission (ASE) and random lasing. Here, a monolayer of such CQW stacks is obtained *via* liquid–air interface self-assembly (LAISA) in a binary subphase by controlling the hydrophilicity/lipophilicity balance (HLB), a critical factor for maintaining the orientation of CQWs during their self-assembly. Ethylene glycol, as a hydrophilic subphase, orients the coalition of these CQWs into self-assembled multi-layers in the vertical direction. Stacking CQWs into large micron-sized areas as a monolayer is facilitated by adjusting HLB with diethylene glycol addition as a more lyophilic subphase during LAISA. ASE was observed from the resulting multi-layered CQW stacks prepared *via* sequential deposition onto the substrate by applying the Langmuir–Schaefer transfer method. Random lasing was achieved from a single self-assembled monolayer of the vertically oriented CQWs. Here, highly rough surfaces resulting from the non-close packing nature of the CQW stack films cause strongly thickness-dependent behavior. We observed that in general a higher roughness-to-thickness ratio of the CQW stack films (*e.g.*, thinner films that are intrinsically rough enough) leads to random lasing, while it is possible to observe ASE only in thick enough films even if their roughness is relatively higher. These findings indicate that the proposed bottom-up technique can be used to construct thickness-tunable, three-dimensional CQW superstructures for fast, low-cost, and large-area fabrication.

Received 11th January 2023,
Accepted 28th April 2023

DOI: 10.1039/d3nr00170a

rsc.li/nanoscale

Introduction

Engineering of colloidal semiconductor nanocrystals (NCs) by controlling their composition, size, shape, and ligands allows the attainment of different electronic and optical properties that emerge from their quantum-confined structures.[1–4] Another complementary approach to modify and control their properties is the self-assembly of these colloids, a phenomenon leading to ordered (or partially ordered) systems resulting in possibly advantageous functional formations and collective behavior from their nano- to macro-sized superstructures.[5] Similar to well-known intriguing examples of self-assemblies such as molecular assemblies of nucleic acids enabling functional DNA constructs[6,7] and assemblies of organic–inorganic molecules giving rise to crystal formation,[8–10] the bottom-up organization of nanocrystals forms interesting superlattices.[11,12]

Such self-assembly of semiconductor nanocrystals is a significant enabler that may dramatically change the collective properties of the resulting NC ensemble.[13–16] For example, honeycomb superlattices obtained from the self-assembly of colloidal PbS quantum dots (QDs) combined with the attachment of these QDs induce strong spin–orbit coupling and generate Dirac-type electronic bands as in graphene; as a result of the attachment, the electron mobility also changes.[17] Similarly, the self-assembly phenomenon is also quite influen-

[a]*Faculty of Engineering, Department of Biomedical Engineering, Eskisehir Osmangazi University, Eskisehir 26040, Turkey*
[b]*Department of Electrical and Electronics Engineering, Department of Physics, UNAM – Institute of Materials Science and Nanotechnology, Bilkent University, Ankara 06800, Turkey. E-mail: volkan@bilkent.edu.tr*
[c]*Sabuncuoglu Serefeddin Health Services Vocational School, Amasya University, Amasya 05100, Türkiye*
[d]*Luminous! Center of Excellence for Semiconductor Lighting and Displays, School of Electrical and Electronic Engineering, Division of Physics and Applied Physics, School of Physical and Mathematical Sciences, School of Materials Science and Engineering, Nanyang Technological University, Singapore 639798, Singapore*
† Electronic supplementary information (ESI) available. See DOI: https://doi.org/10.1039/d3nr00170a

tial on the emerging properties of colloidal quantum wells (CQWs), a quasi-two dimensional sub-family of NCs, which have found important applications in recent years owing to their distinct advantages such as narrow spontaneous emission spectra and large absorption cross-sections.[18–20]

The self-assembly of CQWs into superlattices may enable newly ordered artificial solids for optoelectronic applications. This, however, requires critical orientation control. For example, oriented self-assembly of CQWs allows for long-range energy transfer through vertically oriented CQW chains,[21] strongly polarized emission from the stacks of CQWs assembled in solution,[22,23] and control of the transition dipole moment orientation of laterally oriented CQWs enhancing their light outcoupling efficiency.[22]

Besides managing the emergent material behavior *via* the oriented self-assembly, the reported methods for colloidal self-assembly are also quite preferable compared to conventional top-down techniques (*e.g.*, electron beam lithography) that typically suffer from high-cost, complicated fabrication processes and the requirement of essential costly equipment. At the same time, self-assembly makes the realization of three-dimensional superstructures with sub-nanometer precision for otherwise challenging structural designs possible.[12,15,16,24,25] LAISA, as the most frequently used method, works by managing molecular interactions[26] (dipole–dipole and electrostatic interactions, *etc.*) between CQWs and a subphase *via* ligand exchange,[22] adjusting van der Waals forces between aliphatic chains,[15] and kinetic control *via* the solvent evaporation rate.[27] This controllable nature of self-assembly provides us with the ability to produce an oriented assembly of anisotropic colloidal nanocrystals under certain conditions.[28,29]

Previously, highly organized face-down oriented CdSe/$Cd_{0.25}Zn_{0.75}S$ CQW films that act as optically active planar waveguides were prepared with precise film thickness control *via* LAISA and they allowed for thickness-dependent optical gain and ASE threshold.[16] Since ASE is an effective indicator to compare the material capability for optical gain, the ASE behaviors of different types of colloidal nanocrystals have been investigated.[19,30–33] Such laterally oriented self-assembly of CQWs has paved the way for the development of ultrathin optical gain media with tunable thickness, thanks to the excellent uniformity and close-packed nature of their films.[16]

Herein, different from our previous work, we propose and demonstrate vertically oriented self-assembled monolayer (SAM) film formation of CdSe/CdZnS CQWs by controlling the hydrophilicity/lipophilicity balance of their subphase by using a binary subphase. The addition of a surfactant into the substrate is also shown to be highly effective for controlling the orientation and self-assembly process of these CQWs. The optical gain behavior of the resulting non-close-packed CdSe/CdZnS CQW stacks with different thicknesses is systematically studied. We observe that the roughness of thinner CQW stack films results in random lasing, while thick samples exhibit ASE despite them having greater roughness. The ASE threshold of these non-close-packed stacks produced by sequencing five layers of CdSe/CdZnS CQW SAM is 75 μJ cm^{-2}.

Results and discussion

In this work, CdSe/$Cd_{0.25}Zn_{0.75}S$ core/alloyed shell CQW synthesis was performed *via* seeded growth and hot injection methods by using 4 ML CdSe CQWs as seeds, as reported by our group previously.[34] CQWs with a mean lateral size of 13 ± 3 nm (long side) by 3.5 ± 1 nm (short side) are shown in the transmission electron microscopy (TEM) images (Fig. 1a and Fig. S1†). The absolute photoluminescence quantum yield (PLQY) of these CdSe/$Cd_{0.25}Zn_{0.75}S$ core/alloyed shell CQWs measured at an excitation wavelength of 400 nm using a calibrated integrating sphere is 98%. As shown in the absorption spectrum, two excitonic peaks of the synthesized CQWs are located at 637 and 576 nm, respectively, while their photoluminescence (PL) peaks are at 650 nm (Fig. 1b).

To develop our approach for obtaining edge-up-oriented SAM while discouraging the potential tendency of CdSe/CdZnS CQWs to orient themselves face down, the size, shape, composition, ligand type, and ligand amount (*i.e.*, the effect of ligand removal)[35] on the surface of CQWs need to be carefully considered as the decisive parameters affecting the interactions of CQWs with each other and the subphase. In addition to these parameters related to the nature of CQWs, the solvent type responsible for vapor pressure (evaporation rate) and the solvent amount that enables kinetic control are critical for orientation-controlled self-assembly. As another component of the LAISA, the subphase is also crucial for changing the orientation of the self-assembly of CQWs, as reported before.[22,29] Increasing the hydrophilicity or polarity of the subphase can switch the orientational assembly behavior of CQWs because of reduced interactions of the subphase with the highly apolar CQW surface caused by long aliphatic chains. Excessive increase of the subphase hydrophilicity results in a coalition of CdSe/$Cd_{0.25}Zn_{0.75}S$ CQWs on a specific part of the subphase. This CdSe/$Cd_{0.25}Zn_{0.75}S$ CQW coalition leads to an edge-up orientation caused by the reduced surface contact area of CQWs with the hydrophilic subphase. As a result, the interactions of CQWs between themselves increases because of this repulsive force. Appropriate hydrophilicity may help with the spreading of these stacked CQWs as a monolayer onto the subphase. The use of diethylene glycol (DEG), as the most common subphase, allows for face-down self-assembly, as reported by our group previously,[16] owing to its nonrepulsive hydrophilicity for CdSe/$Cd_{0.25}$ $Zn_{0.75}S$ CQWs.

Therefore, this hydrophilicity difference between the subphase and the CQWs strongly depends on CQW-related parameters (size, shape, ligand, *etc.*). The use of ethylene glycol (EG) as a subphase results in an edge-up oriented coalition of CdSe/$Cd_{0.25}Zn_{0.75}S$ CQWs. Since the spreading of CQWs onto the subphase as a monolayer is not possible because of the high hydrophilicity of EG, the usage of a co-subphase decreasing hydrophilicity (*i.e.*, the inter-surface tension between the ligands of CQWs and the subphase) would enable spreading of the CQWs onto the surface as stacks.

Increasing the chain length of diol subphases such as in ethylene glycol, diethylene glycol (DEG), and triethylene glycol

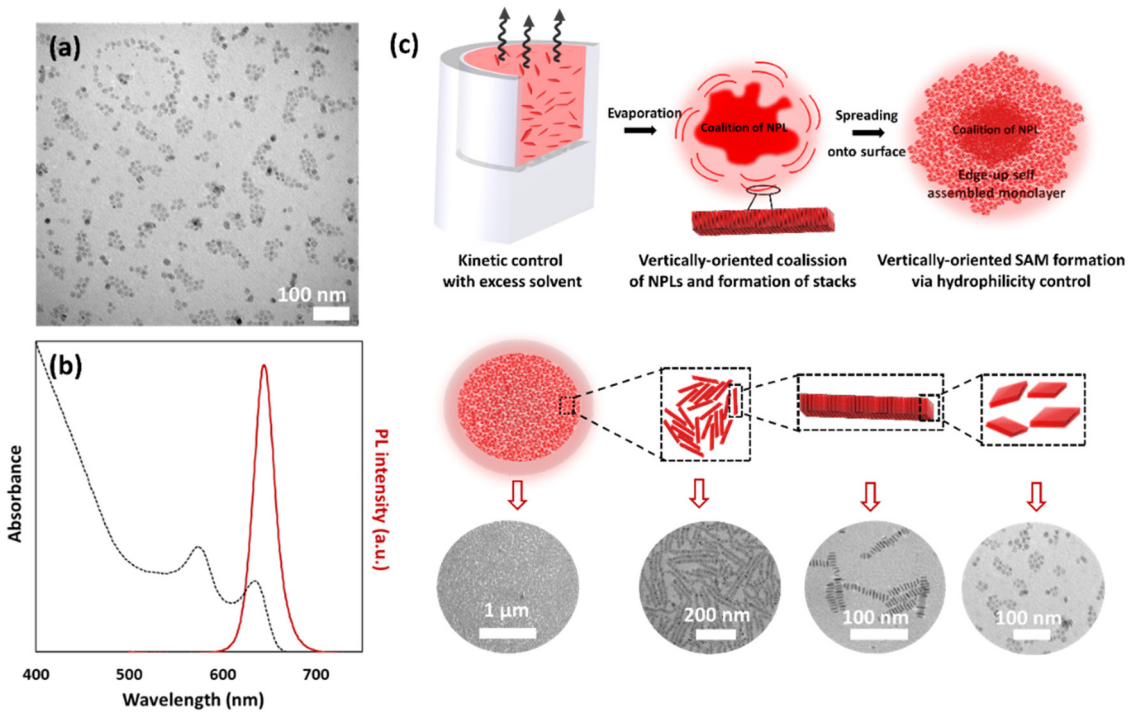

Fig. 1 A transmission electron micrograph of square-shaped CdSe/CdZnS core/shell CQWs (a). Absorbance and photoluminescence spectra for the CdSe/CdZnS CQWs (b). Illustration of edge-up self-assembled monolayer (SAM) formation supported by TEM micrographs (c).

(TEG) decreases hydrophilicity (*i.e.*, hydrophilicity: EG > DEG > TEG).[36,37] The decrease of hydrophilicity (*i.e.*, lipophilic increase) also affects the molecular interactions between the lipophilic ligand-capped CQWs and the subphase. The addition of DEG (or TEG) to the EG subphase spreads the CQW stacks as a monolayer onto the surface while the EG subphase causes the coalition of edge-up oriented stacks. Excessive solvent usage also facilitates both spreading onto the subphase and interactions of CQWs among themselves for the stack formation.

The edge-up-oriented SAM formation is illustrated in Fig. 1c using their TEM micrographs. The use of DEG as a co-subphase is proved to be quite effective with its addition in low percentages, as shown in TEM images (Fig. 2). While the usage of a 5% DEG subphase along with EG as the main subphase results in the stack formation and spreading of CQWs onto the subphase (Fig. 2a), the use of 15% DEG causes a face-down orientation of CQWs (Fig. 2b).

A vertically oriented SAM of CQW stacks on a large scale is formed around the coalition area, as shown in TEM images (Fig. S1c,† Fig. 3a–c and Fig. S1d,† respectively). TEM samples were prepared by taking the layers deliberately from the edges of the coalition area to show a vertically oriented coalition and monolayer formation around it. Even though CQW stacks are not close-packed, all of them are observed to be oriented edge up or positioned at an angle (*i.e.*, neither edge-up nor face-down, see Fig. S1a and b†).

The most common SAM transfer method onto the substrate is to place the substrate in the subphase and slowly drain the subphase with a peristaltic pump.[38]

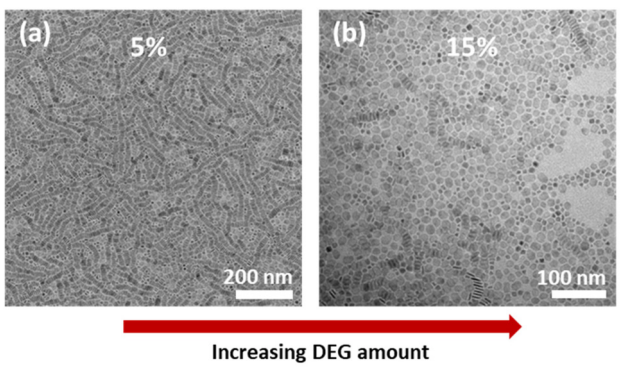

Fig. 2 TEM micrographs of self-assembly layers with increasing DEG co-subphase usage: the CQW stack formation with 5% DEG (a). Stacks and face-down oriented CQW organization with 15% DEG (b).

Since this method is time-consuming, transferring the SAM layers onto the substrate from the top is easier and faster, as depicted in Fig. 3d. While this method, commonly known as the Langmuir–Schaefer transfer method, has been used for transferring a large variety of materials, here we used this approach to move the SAM of CQW stacks onto silicon and silica substrates 1 × 1 cm^2 in size.[39] After sticking the CQW SAM onto the substrate by drying under vacuum for 30 min, the samples were removed and placed on a Petri dish containing acetonitrile (ACN), which does not interact with CQWs and has high vacuum pressure leading to easy drying. After removing excess ethylene glycol of the CQW layer by washing with

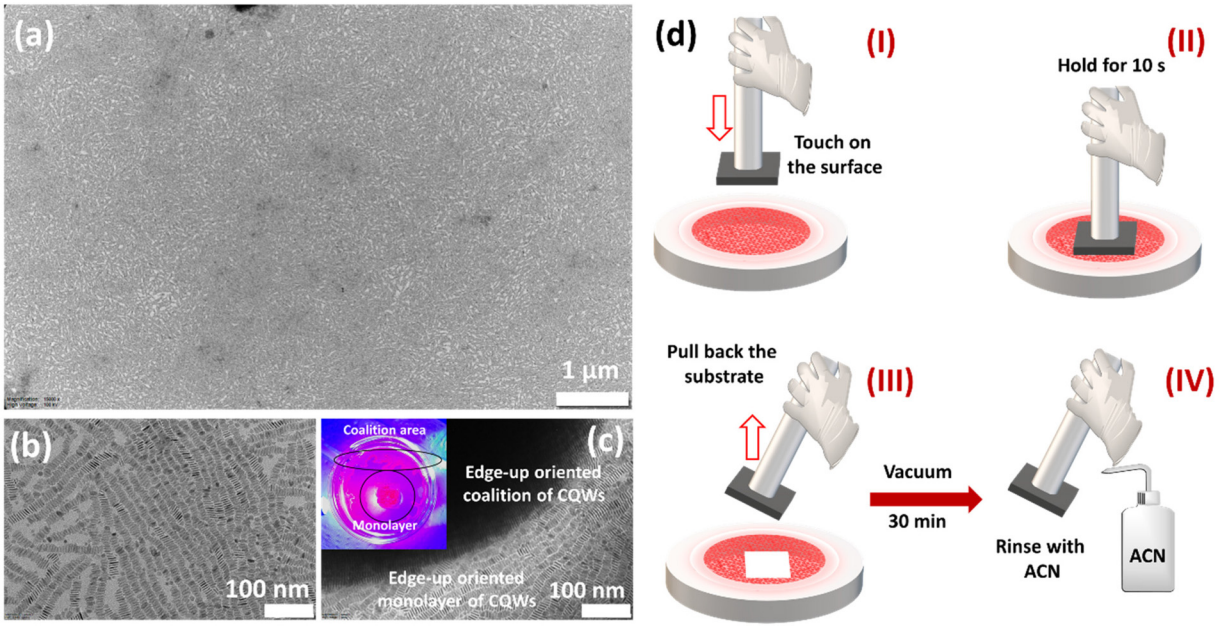

Fig. 3 TEM micrographs of edge-up oriented CQW SAM formation in a micron sized large area (a and b). A coalition of CQWs during self-assembly (c). Illustration of the sample preparation process step by step using the top-picking Langmuir–Schaefer transfer method (d).

ACN, the samples were dried one more time under vacuum. This method can be further improved to obtain films with reduced roughness. For example, using a larger Petri dish (here 35 mm Petri dishes were used) for larger SAM areas may ease both sample picking and multiple picking. The SAM area forming on the subphase (35 mm in diameter) is around 20 mm in diameter, which allows us to pick the sample onto a substrate 1 × 1 cm^2 in size. Also, using a solvent with lower vapor pressure and a substrate with increased hydrophobicity may facilitate the formation of SAM layers with lower roughness.

The self-assembly process with a binary subphase approach to balance lipophilicity also introduces the idea that using surfactants could be functional for adjusting the orientation of CQWs during self-assembly. Even though the effect of oleic acid usage has been reported in the literature, the surfactant effect has not been discussed before.[22] Surfactants with their hydrophobic tail and hydrophilic head can assemble on the surface of the subphase and reduce the surface tension.[40] While adding less surfactant may affect the spreadability of CQWs on the hydrophilic subphase because of lower surface tension, hydrophobic tails also may trigger orientation as face down.

Here we further used cetyltrimethylammonium bromide (CTAB) as a short-tailed hydrophobic surfactant and sodium dodecyl sulfate (SDS) as an extended hydrophobic tailed surfactant to benefit from the effect of the surfactant on the self-assembly. Both surfactants were dissolved in EG, which is a hydrophilic subphase.

The use of CTAB favored the edge-up oriented self-assembly with a low concentration of CQWs, while the SDS usage mainly resulted in the face-down oriented self-assembly (Fig. S2†).

Back focal plane (BFP) imaging patterns were obtained as described in a section in the ESI† both by simulation and experiment to study the dipole orientation of the vertically oriented SAM of CQW stacks (Fig. 4a and b, respectively). Neither the pure in-plane nor out-of-plane emission patterns

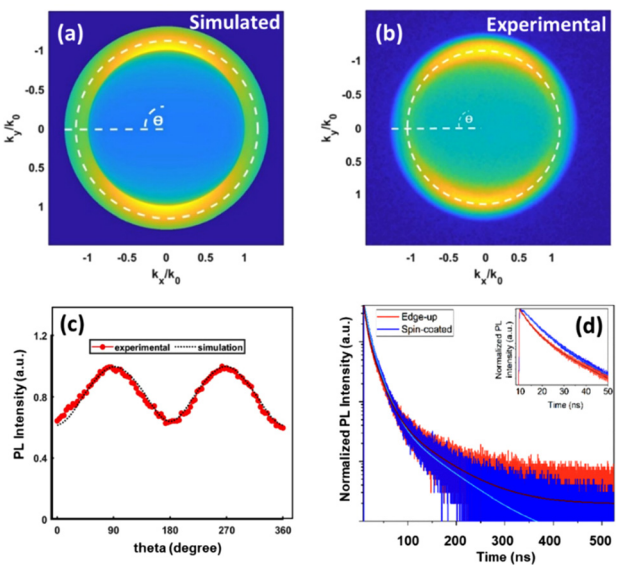

Fig. 4 A simulated BFP image of the case of a 50/50 mixture of in-plane and out-of-plane dipoles, *i.e.*, $R = \mu_a/\mu_b = 1$ (a). An experimental BFP image from the vertically oriented self-assembly (b). Comparison between experimental and simulated line cuts along the circle is indicated by the dashed white lines in panels (c). TRF spectra of edge-up SAM and spin-coated CQW films (d).

resemble that of the edge-up pattern (Fig. S5†). However, the emission pattern may be precisely computed by assuming equal contributions from the in-plane and out-of-plane dipole orientations. In theory, in-plane anisotropy might polarize the dipole along the nanoplatelet's long axis, similar to rods and wires. However, an isotropic dipole distribution within the nanoplatelet plane best fits the intensity graph.

Because the nanoplatelets are stacked on their long edges in the vertical orientation, aligning the dipole along the nanoplatelet's long axis produces a BFP pattern similar to that in the in-plane. We fitted multiple combinations of long-axis and short-axis dipole contributions for the edge-up construction to quantify further the orientation distribution of dipoles in the CQW plane. According to the simulation findings, the ratio of long-axis to short-axis dipole contribution is one, as seen in the intensity diagram (Fig. 4c).

Time-resolved fluorescence (TRF) decay curves of two films, one prepared through self-assembly of the CQWs as vertically oriented and the other one by spin-coating, are demonstrated in Fig. 4d. The curves were fitted with three-exponential functions, in line with previous reports in the literature for core/shell CQWs.[41,42] Both samples demonstrate close intensity-average lifetimes (τ_{avg}) with a slight change in their lifetime components and fractional intensities of each channel (Table S1†).

For the vertically oriented CQW film, as the distance between the CQWs is reduced to the shortest proximity in the order of the ligand length while increasing the surface contact area of the CQWs in the neighborhood, the chance of a non-radiative energy transfer process is increased. The process involves a donor-to-acceptor coupling, where besides the distance of the donor and acceptor, it depends on the relative orientation of the CQWs, the PLQY of the donor, and the spectral overlap of the absorption of the acceptor and the PL of the donor, respectively.[43,44] In our case study, the overlap is limited to a tiny area of the PL and absorption on the one hand, and the CQWs are closely packed in a face-to-face orientation on the other. Thus, the slight decrease in the shortest lifetime component, which conventionally possesses more non-radiative characteristics, is apparent. For a spin-coated CQW film, the effective distance of the CQWs is increased, which provides a higher chance of radiative energy transfer through the reabsorption of the emitted photons.

Moreover, the number of CQWs is much higher than that in the case of one layer of the self-assembled film. Hence, the spin-coated CQW film demonstrates a lower fractional intensity of the shortest channel and the highest fraction for the longest one. Hence, the spin-coated sample exhibits a lower fractional emission contribution from the fastest channel (12%, compared to 15% of the edge-up sample) and a higher fraction for the slowest one (63%, compared to 60% of the edge-up sample). The corresponding lifetimes are 20.8 and 21.9 ns for the spin-coated and edge-up films, respectively.

Optical gain studies of the vertically oriented CQW films were performed with increasing sequential deposition numbers of the CQW stack films (n) onto a fused silica substrate, up to n = 10. As a result of our systematic study, the vertically oriented CQW films with n = 4 and above exhibited ASE (Fig. S6†). Fig. 5a presents sequentially deposited films of

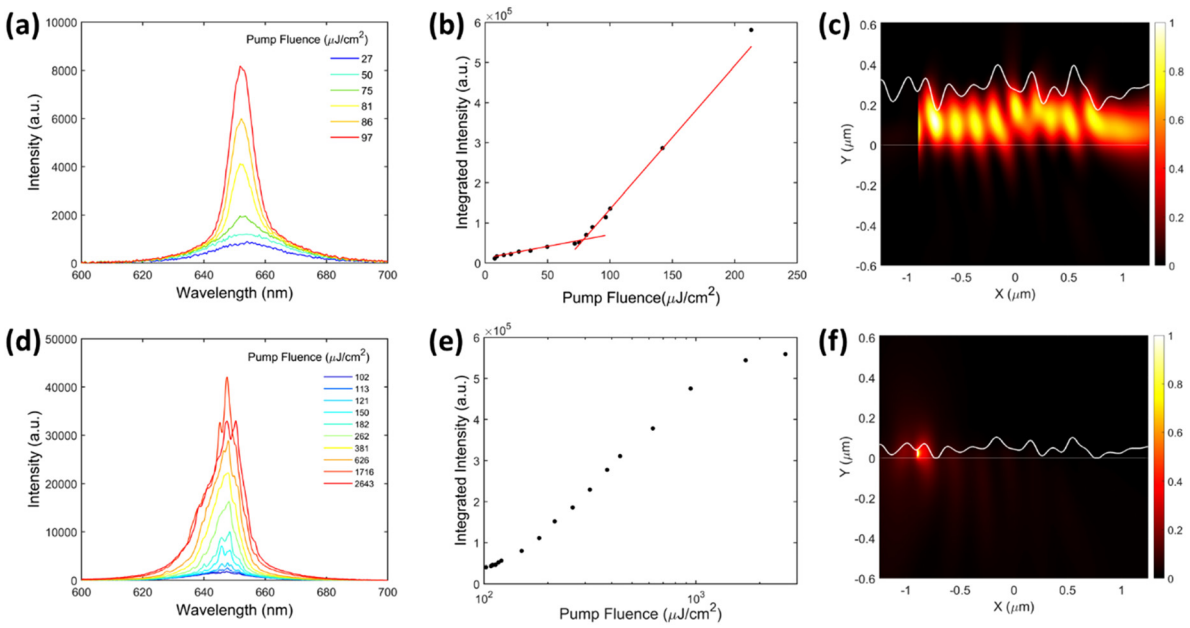

Fig. 5 PL spectral evolution of the edge-up oriented CdSe/CdZnS CQW film (n = 5) under single-photon excitation (λ_{exc} = 400 nm) shown for the different pulse energy densities of the pump (a). Integrated emission intensity as a function of the pump fluence (b). The electric field intensity for a CQW film with a thickness of 225 nm and an RMS roughness of 55 nm (c). PL spectra evolution of the edge-up oriented CdSe/CdZnS CQWs monolayer film (n = 1) under single-photon excitation (λ_{exc} = 400 nm) shown for the different pulse energy densities of the pump (d). Integrated emission intensity as a function of the pump fluence (e). The electric field intensity for a CQW film with a thickness of 46 nm and an RMS roughness of 26 nm (f).

CQW stacks with n = 5 corresponding to a film thickness of 65 nm determined by optical profilometer measurements. The stripe excitation configuration was utilized for the ASE measurements, where the pump excitation was incident on the sample, and the PL emission was collected from the edge. The incident pump had a 400 nm wavelength with a 1 kHz pulse rate and an ~110 fs pulse width. The PL spectra were collected at different pump fluences. ASE was characterized by the emergence of the second emission feature above a pumping threshold and the spectral narrowing and change in the slope of the integrated emission intensity (Fig. 5b). The per pulse gain threshold for the sample with n = 5 was 78.5 μJ cm^{-2}.

Here, vertically oriented monolayer CQW films and films with n < 4 exhibited random lasing, as shown in Fig. 5d and Fig. S6a,† and the integrated emission intensity-pump fluence graph is given in Fig. 5e. As characteristic behavior of random lasing mode, the position and spectral range between peaks change on increasing the pump fluence. We propose that a random lasing mode is created by virtue of the roughness on the surface of CQW stack films as determined by AFM topology imaging and roughness measurements (Fig. S7†). It creates a random grating structure of the CQW film on a fused silica substrate, with a high refractive index variation between the CQW film (1.9) and air (1). There are many challenges in obtaining random lasing as strong scattering and high optical gain have to be achieved simultaneously. Here, the vertical orientation of CQW films results in a high density of active centers compared to face-down or spin-coated films with a random direction in the same excitation area, which increases the maximum achievable modal gain contributing positively to random lasing. To develop understanding of the lasing behavior of our self-assembled stack CQW films, we performed a full electro-magnetic computation using the finite-difference time-domain method *via* a commercial software package (numerical finite-difference time-domain solutions).

Our numerical solution modeled the gain media with an optical refractive index (n_{CQW}) of 1.90, according to our experimental characterization *via* the ellipsometry technique. Fig. 5c shows that the electric field is effectively guided along the film despite high roughness for a thick CQW film with a thickness of 225 nm and a roughness of 55 nm. Meanwhile, as shown in Fig. 5f, for a thin CQW film with a thickness of 46 nm and a roughness of 26 nm, a large fraction of the electric field is reflected compared to a thicker film.

Table 1 summarizes the computational results for three different samples. These results show that in thinner films of stacked CQWs, the emitted light from CQWs undergoes multiple random scattering at the high-density CQW boundaries. The photons can be trapped in a scattering path in this process, forming random closed-loop cavities.

Table 1 Thickness, RMS roughness, and reflectance values of CQW stack films

n	Thickness (nm)	RMS roughness (nm)	Reflectance (%)
1	16	19.2 ± 5.8	12
3	46	26.4 ± 13.1	11
10	225	54.7 ± 13.4	6

Conclusions

In conclusion, we demonstrated orientational control over CdSe/CdZnS CQW self-assembly as vertically oriented by adjusting hydrophilicity with a binary subphase and also surface tension with surfactant addition to the subphase. Since stacks of CQWs prepared by the hydrophilicity/lipophilicity balance method are not closely packed, highly rough surfaces are obtained compared to face-down self-assembled films. The roughness of the vertically oriented films has a decisive effect on optical gain behavior, changing from random lasing to ASE, depending on the thickness of sequentially deposited films. Even though random lasing is observed with the thin films (n = 1 to 3) with high roughness, optical gain behavior changed to ASE with thicker films ($n \geq 4$) even if the roughness is much higher, resulting from the waveguiding effect in this case. Orientational control over the self-assembly of CdSe/CdZnS CQWs is crucial because of their unique emerging properties that can pave the way for many applications such as orientationally designed CQW LEDs, lasers, and other optical devices.

Author contributions

Dikmen Z: methodology, conceptualization, data curation, writing of the original draft, review & editing, and funding acquisition; Işık A. T.: data curation and methodology; Bozkaya İ.: data curation and methodology; Canımkurbey B.: data curation; Shabani F.: data curation; Ahmad M.: data curation; Demir H. V.: project administration, resources, supervision, conceptualization, visualization, funding acquisition, and writing, review & editing of the manuscript.

Conflicts of interest

There are no conflicts to declare.

Acknowledgements

The authors gratefully acknowledge the financial support from TUBITAK 119N343, 20AG001, 121N395 and 121C266. Z. D. acknowledges financial support from the Scientific and Technological Research Council of Turkey (TUBITAK), GN: 120Z259 and 118C517. B. C. acknowledges financial support from the Scientific and Technological Research Council of Turkey (TUBITAK), GN: 120C219. We are also thankful to Mr Sina Foroutan Barenji for valuable assistance in optical gain measurements. H. V. D. acknowledges the support from TÜBA.

References

1 J. van Embden, A. S. R. Chesman and J. J. Jasieniak, *Chem. Mater.*, 2015, **27**, 2246–2285.
2 C. D. M. Donegá, *Chem. Soc. Rev.*, 2011, **40**, 1512–1546.
3 K. De Nolf, R. K. Capek, S. Abe, M. Sluydts, Y. Jang, J. C. Martins, S. Cottenier, E. Lifshitz and Z. Hens, *J. Am. Chem. Soc.*, 2015, **137**, 2495–2505.
4 D. V. Talapin, J. H. Nelson, E. V. Shevchenko, S. Aloni, B. Sadtler and A. P. Alivisatos, *Nano Lett.*, 2007, **7**, 2951–2959.
5 B. A. Grzybowski, C. E. Wilmer, J. Kim, K. P. Browne and K. J. M. Bishop, *Soft Matter*, 2009, **5**, 1110–1128.
6 A. Lazcano, *ACS Nano*, 2018, **12**, 9643–9647.
7 C. K. McLaughlin, G. D. Hamblin and H. F. Sleiman, *Chem. Soc. Rev.*, 2011, **40**, 5647–5656.
8 H. Chen, M. Li, Z. Lu, X. Wang, J. Yang, Z. Wang, F. Zhang, C. Gu, W. Zhang, Y. Sun, J. Sun, W. Zhu and X. Guo, *Nat. Commun.*, 2019, **10**, 3872.
9 L. Zang, Y. Che and J. S. Moore, *Acc. Chem. Res.*, 2008, **41**, 1596–1608.
10 K. Harano, *Bull. Chem. Soc. Jpn.*, 2021, **94**, 463–472.
11 A. Dong, J. Chen, P. M. Vora, J. M. Kikkawa and C. B. Murray, *Nature*, 2010, **466**, 474–477.
12 D. Vanmaekelbergh, *Nano Today*, 2011, **6**, 419–437.
13 M. Zavelani-Rossi, M. G. Lupo, R. Krahne, L. Manna and G. Lanzani, *Nanoscale*, 2010, **2**, 931–935.
14 M. D. Tessier, L. Biadala, C. Bouet, S. Ithurria, B. Abecassis and B. Dubertret, *ACS Nano*, 2013, **7**, 3332–3340.
15 M. A. Boles, M. Engel and D. V. Talapin, *Chem. Rev.*, 2016, **116**, 11220–11289.
16 O. Erdem, S. Foroutan, N. Gheshlaghi, B. Guzelturk, Y. Altintas and H. V. Demir, *Nano Lett.*, 2020, **20**, 6459–6465.
17 M. P. Boneschanscher, W. H. Evers, J. J. Geuchies, T. Altantzis, B. Goris, F. T. Rabouw, S. A. P. van Rossum, H. S. J. van der Zant, L. D. A. Siebbeles, G. Van Tendeloo, I. Swart, J. Hilhorst, A. V. Petukhov, S. Bals and D. Vanmaekelbergh, *Science*, 2014, **344**, 1377–1380.
18 A. Yeltik, S. Delikanli, M. Olutas, Y. Kelestemur, B. Guzelturk and H. V. Demir, *J. Phys. Chem. C*, 2015, **119**, 26768–26775.
19 B. Guzelturk, Y. Kelestemur, M. Olutas, S. Delikanli and H. V. Demir, *ACS Nano*, 2014, **8**, 6599–6605.
20 S. Delikanli, O. Erdem, F. Isik, H. Dehghanpour Baruj, F. Shabani, H. B. Yagci, E. G. Durmusoglu and H. V. Demir, *J. Phys. Chem. Lett.*, 2021, **12**, 2177–2182.
21 J. W. Liu, L. Guillemeney, B. Abecassis and L. Coolen, *Nano Lett.*, 2020, **20**, 3465–3470.
22 Y. N. Gao, M. C. Weidman and W. A. Tisdale, *Nano Lett.*, 2017, **17**, 3837–3843.
23 B. Abecassis, M. D. Tessier, P. Davidson and B. Dubertret, *Nano Lett.*, 2014, **14**, 710–715.
24 F. Montanarella, D. Urbonas, L. Chadwick, P. G. Moerman, P. J. Baesjou, R. F. Mahrt, A. van Blaaderen, T. Stöferle and D. Vanmaekelbergh, *ACS Nano*, 2018, **12**, 12788–12794.
25 B. A. Parviz, D. Ryan and G. M. Whitesides, *IEEE Trans. Adv. Packag.*, 2003, **26**, 233–241.
26 B. Abécassis, *ChemPhysChem*, 2016, **17**, 618–631.
27 R. Momper, H. Zhang, S. Chen, H. Halim, E. Johannes, S. Yordanov, D. Braga, B. Blulle, D. Doblas, T. Kraus, M. Bonn, H. I. Wang and A. Riedinger, *Nano Lett.*, 2020, **20**, 4102–4110.
28 F. Pietra, F. T. Rabouw, W. H. Evers, D. V. Byelov, A. V. Petukhov, C. de Mello Donegá and D. Vanmaekelbergh, *Nano Lett.*, 2012, **12**, 5515–5523.
29 O. Erdem, K. Gungor, B. Guzelturk, I. Tanriover, M. Sak, M. Olutas, D. Dede, Y. Kelestemur and H. V. Demir, *Nano Lett.*, 2019, **19**, 4297–4305.
30 S. Yakunin, L. Protesescu, F. Krieg, M. I. Bodnarchuk, G. Nedelcu, M. Humer, G. De Luca, M. Fiebig, W. Heiss and M. V. Kovalenko, *Nat. Commun.*, 2015, **6**, 8056.
31 D. O. Kundys, P. Murzyn, J.-P. R. Wells, A. I. Tartakovskii, M. S. Skolnick, L. S. Dang, E. V. Lutsenko, N. P. Tarasuk, O. G. Lyublinskaya, A. A. Toropov and S. V. Ivanov, *J. Appl. Phys.*, 2006, **100**, 123510.
32 H. Htoon, J. A. Hollingworth, A. V. Malko, R. Dickerson and V. I. Klimov, *Appl. Phys. Lett.*, 2003, **82**, 4776–4778.
33 V. I. Klimov, A. A. Mikhailovsky, S. Xu, A. Malko, J. A. Hollingsworth, C. A. Leatherdale, H.-J. Eisler and M. G. Bawendi, *Science*, 2000, **290**, 314–317.
34 Y. Altintas, K. Gungor, Y. Gao, M. Sak, U. Quliyeva, G. Bappi, E. Mutlugun, E. H. Sargent and H. V. Demir, *ACS Nano*, 2019, **13**, 10662–10670.
35 A. Antanovich, A. Prudnikau, A. Matsukovich, A. Achtstein and M. Artemyev, *J. Phys. Chem. C*, 2016, **120**, 5764–5775.
36 L. Marszall and J. W. Van Valkenburg, *J. Am. Oil Chem. Soc.*, 1982, **59**, 84–87.
37 M. Cachile and A. M. Cazabat, *Langmuir*, 1999, **15**, 1515–1521.
38 S. Foroutan-Barenji, O. Erdem, N. Gheshlaghi, Y. Altintas and H. V. Demir, *Small*, 2020, **16**, 2004304.
39 D. Liu, W. Cai, M. Marin, Y. Yin and Y. Li, *ChemNanoMat*, 2019, **5**, 1338–1360.
40 J. Bergfreund, P. Bertsch and P. Fischer, *Curr. Opin. Colloid Interface Sci.*, 2021, **56**, 101509.
41 M. Pelton, J. J. Andrews, I. Fedin, D. V. Talapin, H. Leng and S. K. O'Leary, *Nano Lett.*, 2017, **17**, 6900–6906.
42 F. Shabani, H. Dehghanpour Baruj, I. Yurdakul, S. Delikanli, N. Gheshlaghi, F. Isik, B. Liu, Y. Altintas, B. Canımkurbey and H. V. Demir, *Small*, 2022, **18**, 2106115.
43 C. Bradac, Z.-Q. Xu and I. Aharonovich, *Nano Lett.*, 2021, **21**, 1193–1204.
44 S. Panuganti, L. V. Besteiro, E. S. Vasileiadou, J. M. Hoffman, A. O. Govorov, S. K. Gray, M. G. Kanatzidis and R. D. Schaller, *J. Am. Chem. Soc.*, 2021, **143**, 4244–4252.